Research Square

Preprints are preliminary reports that have not undergone peer review.
They should not be considered conclusive, used to inform clinical practice,
or referenced by the media as validated information.

Hyperspectral Imaging for Subsurface Mineral Characterization: Integrated Application with FLEX Log and XRD in Devonian Ouabed reservoirs - Algeria

Ali Seyfeddine Guenaoui

a.guenaoui@uni-boumerdes.dz

University of Boumerdes

Omar Bakeli

University of Utah

Khaled Benyounes

University of Boumerdes

Hamid Lebtahi

University of Boumerdes

Ahlam Laouar

University of Ouargla

Ramzi Fellah

University of Ouargla

Research Article

Keywords: Hyperspectral imaging, Clay minerals, X-ray Diffraction (XRD), Clay disturbance

Posted Date: November 9th, 2026

DOI: https://doi.org/10.21203/rs.3.rs-11305719/v1

License: This work is licensed under a Creative Commons Attribution 4.0 International License.
Read Full License

Additional Declarations: No competing interests reported.

Hyperspectral Imaging for Subsurface Mineral Characterization: Integrated Application with FLEX Log and XRD in Devonian Ouabed reservoirs - Algeria

Ali Seyfeddine Guenaoui*[1], Omar Bakeli[2], Khaled Benyounes[2], Hamid Lebtahi[2], Ahlam Laouar[2], Ramzi Fellah[2]

Physical Engineering of Hydrocarbons Laboratory, Faculty of Hydrocarbon and Chemistry, University M'Hamed Bougara Boumerdes, Algeria
Laboratory of underground oil, gas, and aquifer reservoirs, Faculty of Hydrocarbons, Renewable Energies, Earth and Universe Sciences, Kasdi Merbah University of Ouargla, Algeria
**Corresponding author. E-mail: a.guenaoui@uni-boumerdes.dz*

Abstract

Clay minerals pose significant challenges in hydrocarbon reservoirs, especially during drilling and production, where clay swelling and migration, particularly from smectite, kaolinite, and illite, can lead to severe operational problems such as stuck pipe and restricted production flow. Several techniques have been used to detect and characterize clay types in subsurface formations, including logging tools and X-ray Diffraction (XRD), but these methods differ in precision, processing time, and operational complexity.

In the Devonian Ouabed reservoirs in Algeria, previous studies have revealed high clay contents with variable mineralogical compositions, which have caused numerous drilling and production difficulties. To identify appropriate solutions for these clay-related issues, two core samples from Wells A and B were analyzed using the FLEX logging tool, XRD, and, for the first time in Algeria, a hyperspectral camera system for clay determination.

Results show distinct mineralogical profiles among the three methods. In Well A, hyperspectral imaging measured 11% kaolinite and 7% illite, aligning with XRD data that indicated a predominantly kaolinitic composition (65%). Conversely, Well B exhibited 15% kaolinite, 9% illite, and 32% mica based on hyperspectral imaging.

Overall, this comparative study shows that hyperspectral imaging delivers rapid, high-resolution clay identification and becomes highly effective when integrated with XRD and logging data.

Keywords: Hyperspectral imaging, Clay minerals, X-ray Diffraction (XRD), Clay disturbance.

1. Introduction

Clay minerals are widely recognized as one of the main factors influencing reservoir quality, especially in sandstone formations. Their presence can cause a range of issues such as permeability reduction, porosity loss, and formation damage due to swelling, dispersion, or migration under certain drilling and production conditions. These effects are particularly critical in formations like the Lower Devonian, which are known to contain various types of clay with complex distributions.

The influence of clay minerals on reservoir quality has been widely studied due to their role in formation damage, porosity loss, and permeability reduction. Clay minerals such as kaolinite, illite, chlorite, and smectite exhibit different behaviors during drilling and production operations. Swelling clays (e.g., smectite and mixed-layer illite-smectite) are known to cause pore blockage, while even non-swelling clays (e.g., kaolinite) can migrate and reduce permeability by clogging pore throats (Pittman, 1992; Wilson & Pittman, 1977).

Several authors have emphasized the impact of clay distribution and structure on hydrocarbon recovery. Chilingar and Vorabutr (1981) classified clay-related reservoir damage mechanisms, linking specific mineral types to capillary sealing, fines migration, and wettability changes. In the Devonian reservoirs of North Africa, El-Toukhy et al. (2013) highlighted that illitic and kaolinitic assemblages often dominate and are associated with severe reduction in permeability in otherwise good quality sandstones.

X-ray Diffraction (XRD) remains the standard technique for identifying and quantifying clay minerals in core samples (Moore & Reynolds, 1997). It allows detection of crystalline phases with relatively high accuracy. However, it requires destructive sampling and does not capture mineralogical variability at fine spatial scales. Ramezanianpour et al. (2012) showed that XRD results need to be interpreted alongside thin section and SEM analysis for better reservoir characterization.

To complement lab-based techniques, downhole logging tools such as the FLEX tool and Spectral Gamma Ray logs are used to estimate total clay volume and differentiate between clay types indirectly. These tools provide continuous data but often lack specificity. Rider and Kennedy (2011) noted that gamma ray responses cannot distinguish between kaolinite and smectite, leading to potential misinterpretation in mixed-lithology intervals. When combined with elemental capture

spectroscopy (ECS) or dielectric logs, log-based clay typing improves but remains limited (Quirein et al., 2007).

In recent years, Hyperspectral Imaging (HSI) has emerged as a non-destructive, high-resolution technique for surface mineral analysis. HSI captures reflectance in the VNIR and SWIR ranges (350 - 2500 nm), allowing for spectral identification of clays and other alteration minerals. Clark et al. (2003) and Turner (2014) demonstrated the potential of HSI in mineral mapping in mining and geotechnical projects. In petroleum applications, Gale et al. (2017) used hyperspectral imaging to characterize fracture fills and diagenetic clays in shale plays. More recently, Berger et al. (2019) applied HSI to study tight sandstone reservoirs, noting that mineral maps helped predict flow behavior.

Despite its demonstrated utility, the application of HSI in conventional petroleum reservoirs especially in the North African context, remains limited. To date, very few studies have directly compared hyperspectral results with those obtained from XRD and wireline logs in the same geological interval. This limits the understanding of how well hyperspectral imaging performs under real reservoir conditions and whether it can be relied upon as a standalone or complementary technique.

This study addresses that gap by conducting a comparative analysis of XRD, FLEX logging, and hyperspectral imaging results as first time application in Algeria in two wells drilled in the Gedinnean formation in the El Ouabed region of Algeria (**Figure 1**) as it shows the presence of a high percentage of clay with different type which directly effects the production. Both wells targeted the Lower Devonian formations including the Emsian, Siegenian, Gedinnean, and Ordovician units. However, the drilling operations encountered multiple complications such as structural irregularities, mud losses, casing failures, stuck pipe events, and wellbore instability. These challenges, combined with the presence of swelling and migrating clay, negatively impacted the porosity and permeability of the reservoir by blocking pore throats and reducing fluid mobility.

- Well A, which specifically targeted the Lower Devonian formations and utilized Oil-Based Mud (OBM) as the drilling fluid, did not demonstrate significant potential for commercial oil accumulation. In contrast, the M'Kratta Formation displayed promising signs of petroleum interest, featuring a 4-meter net pay zone. However, the presence of a substantial volume of clay within the formation posed a significant limitation on permeability. Due to these factors, it was decided to permanently abandon well A.

Well B, focusing on the exploration of the Lower Devonian formations, proved to be productive**,** yielding approximately 2.2 cubic meters. In this case, the drilling fluid used was KCL polymer when reaching the reservoir target. However, the reservoirs within the Lower Devonian formations exhibited mediocre permeability and porosity characteristics due to the presence of clay. This clay content posed limitations on the efficient flow of hydrocarbons.

The main objective of this study is to evaluate the contribution of hyperspectral imaging in identifying and quantifying clay minerals in the Gedinnean reservoir of the El Ouabed region, and to compare its performance with conventional methods, namely X-ray Diffraction (XRD) and the FLEX logging tool. Through this comparison, the study aims to:

- Understand the clay mineral distribution in wells A and B;
- Investigate how clay content and type contribute to permeability loss and production decline;
- Assess whether hyperspectral imaging can provide additional insight into formation damage mechanisms;
- Support future reservoir evaluation and well planning in clay-sensitive formations.

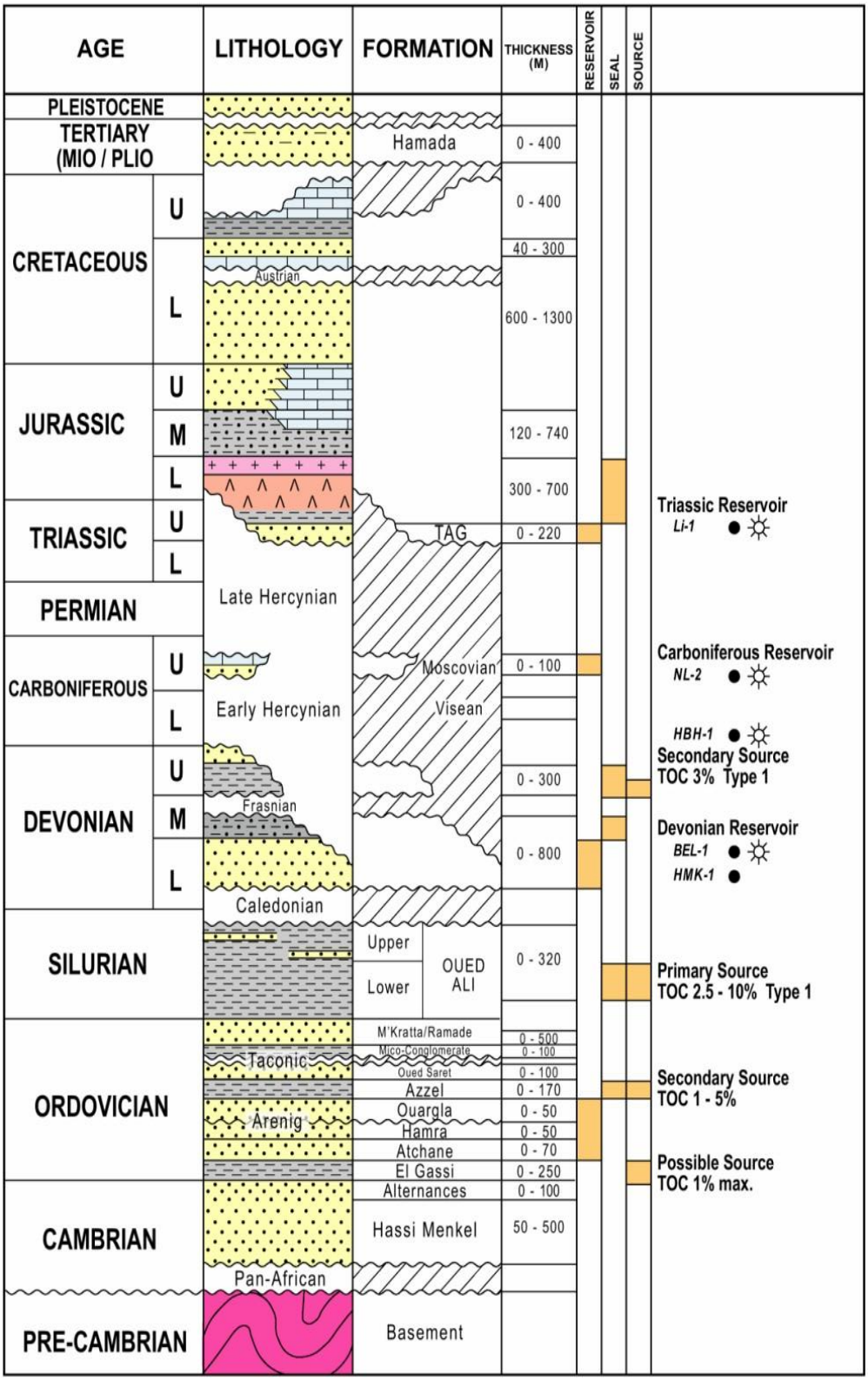


Figure 1 Lithostratigraphic column of the study area.

2. Experimental

2.1. Formation Lithology Explorer (FLEX)

To characterize the mineralogical composition of the Gedinnean reservoir in the El Ouabed field, with a focus on clay minerals affecting well productivity, the Formation Lithology Explorer (FLEX) tool was employed during open hole logging. FLEX is a neutron-induced gamma ray spectroscopy device designed to provide real-time elemental analysis under downhole conditions.

The tool emits pulsed 14 MeV neutrons, which interact with formation nuclei through inelastic scattering and thermal neutron capture. These interactions produce gamma rays characteristic of specific elements. The emitted gamma spectra are captured by a Bismuth Germanate Oxide (BGO) detector, selected for its high energy resolution and efficiency. The detector is shielded with a boron-coated sleeve to reduce thermal noise, allowing for accurate spectral acquisition in high-temperature and high-pressure environments (up to 177°C). The FLEX tool has an outer diameter of 4.87 inches, making it compatible with typical Algerian Devonian wells.

Elemental data primarily: Si, Al, Ca, Fe, K, and Mg, are processed in real time using RockView software to generate mineralogical logs. These logs enable the identification of clay types such as illite, smectite, kaolinite, and chlorite, which are critical for evaluating formation damage potential, permeability reduction, and wellbore stability (Grau & Schweitzer, 1990; Gardner et al., 1997).

2.2. Olympus XRD system

To confirm and complement the mineralogical interpretation obtained from FLEX spectroscopy, X-ray diffraction (XRD) analysis was performed on selected rock samples recovered from specific depth intervals of interest (**Figure 2**). These samples were collected from the intervals 3306 - 3307 m for Well A and 3120 - 3121 m for Well B, which were identified as critical zones in terms of lithological variability and clay concentration during the well logging campaign.

X-ray Diffraction (XRD) analysis was conducted using an Olympus XRD system. This technique is essential for identifying and quantifying clay minerals due to its ability to reveal the crystalline structure and interatomic spacings unique to each mineral type.



Figure 2 Core Samples from Wells A and B for XRD Analysis

The samples were crushed and sieved to obtain fine powders suitable for analysis. The Olympus diffractometer operated with Cu Kα radiation (λ = 1.5418 Å), and the scanning was performed over a 2θ range of 5° to 55°. This range encompasses the principal diffraction peaks of the most common clay minerals, such as kaolinite (7.15 Å, ~12.4° 2θ) and illite (~10 Å, ~8.8° 2θ), both of which were identified in the results.

However, it is important to acknowledge one methodological limitation: the identification of expandable clays such as smectite can be hindered under certain conditions. Although smectite's basal reflection (~15 Å, ~5.8° 2θ) technically falls within the scanned range, its detection often requires specific sample preparation techniques (e.g., ethylene glycol treatment or oriented mounts) due to its tendency to collapse upon drying, leading to peak shifts or suppression (Moore and Reynolds, 1997). Since the standard preparation protocol was used in this study, the confident detection of smectite remains limited, although this does not significantly affect the broader clay classification objective of the research.

The diffraction patterns were processed using the X'Pert HighScore Plus software, and mineral phases were identified by matching peak positions and intensities against the ICDD database.

2.3. Hyperspectral Imaging (VNIR/SWIR Spectroscopy)

To complement the mineralogical information obtained through X-ray diffraction (XRD) and to achieve a high-resolution spatial mapping of clay and associated minerals, hyperspectral imaging (HSI) was employed using the SpecCam 4 hyperspectral imaging system (**Figure 3**). This system integrates Visible-Near Infrared (VNIR) and Short-Wave Infrared (SWIR) sensors, allowing for precise detection of diagnostic absorption features associated with clay minerals and other lithologic components within the 400 - 2500 nm spectral range. This technique allows for the detection of

vibrational molecular bonds and their overtones, generating absorption spectra characteristic of specific mineralogical and hydrocarbon components (Clark, 1999; Kruse, 2012).

Hyperspectral imaging is a non-destructive surface analysis method that measures the vibrational absorptions of molecular bonds (e.g., OH^-, Al-OH, Mg-OH) and their overtones, which manifest as characteristic reflectance features in mineral spectra. These features vary in position, depth, and shape, and are directly linked to mineral composition, crystallinity, hydration state, and cation substitution. This makes HSI particularly valuable for detecting both crystalline and amorphous phases, including illite, kaolinite, chlorite, smectite, and hydrocarbons, even when they occur as fine-grained mixtures or coatings. Unlike traditional mineralogical techniques, this method provides semi-quantitative maps and spectral logs that facilitate the integration of mineralogical composition with lithological interpretation (Van der Meer et al., 2012).

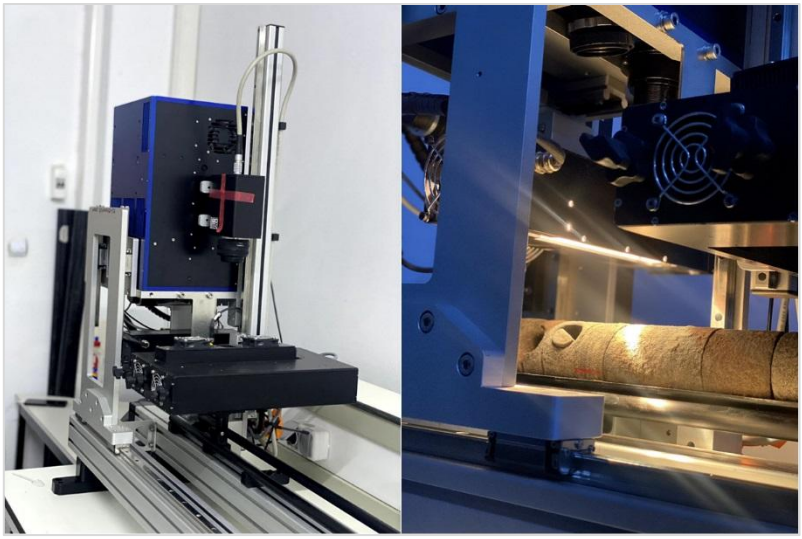


Figure 3 The hyperspectral camera SpecCam 4 Imaging system used.

Two 1-meter core samples were selected from the Gedinnean reservoir in wells A and B (**Figure 4**) based on lithological interpretation from the master log and total vertical depth (TVD). The selected intervals were: Well A: 3306 m to 3307 m and Well B: 3120 m to 3121 m. The cores were cleaned and air dried at an ambient temperature to remove surface contaminants. No coating or chemical treatment was applied to preserve surface spectral integrity.



Figure 4 Core Samples for Hyperspectral Analysis: Well A and Well B.

The SpecCam 4 system is equipped with dual sensors covering both the visible-near infrared (VNIR) and short-wave infrared (SWIR) spectral ranges. The VNIR sensor operates between 400 and 1000 nm with a spectral resolution of approximately 5 - 10 nm, while the SWIR sensor spans 1000 to 2500 nm with a resolution of about 10 - 15 nm (**Figure 5**). A spatial resolution of ~ 0.3 mm per pixel was employed, enabling the detection of fine mineralogical variations at sub centimeter scale. Instrument calibration was carried out using a Spectralon white reference panel to correct for illumination inconsistencies and sensor drift. In addition, internal wavelength calibration was verified using known spectral standards. The system's lighting configuration and sensor alignment were carefully adjusted to eliminate shadows and glare, ensuring uniform illumination and optimal data quality across the entire scanned surface.

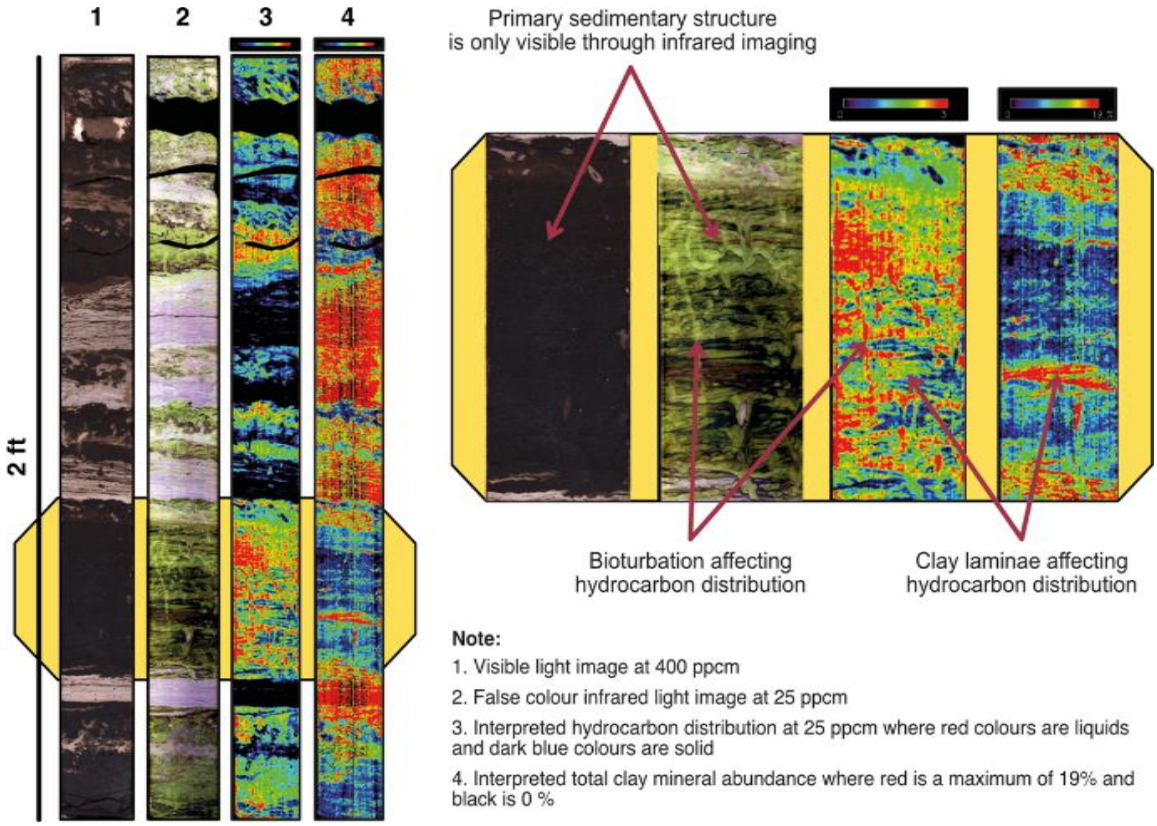


Figure 5 Example SWIR dataset from SpecCam 4 VNIR and SWIR Hyperspectral Spectrometer from an oil sand .

The output included pixel wise mineral classification maps, mineral abundance logs, and hydrocarbon signatures, all essential for improving the lithofacies description and constraining the diagenetic history of the reservoir. Interpretation was performed with the assistance of a trained spectroscopist as part of the software support package.

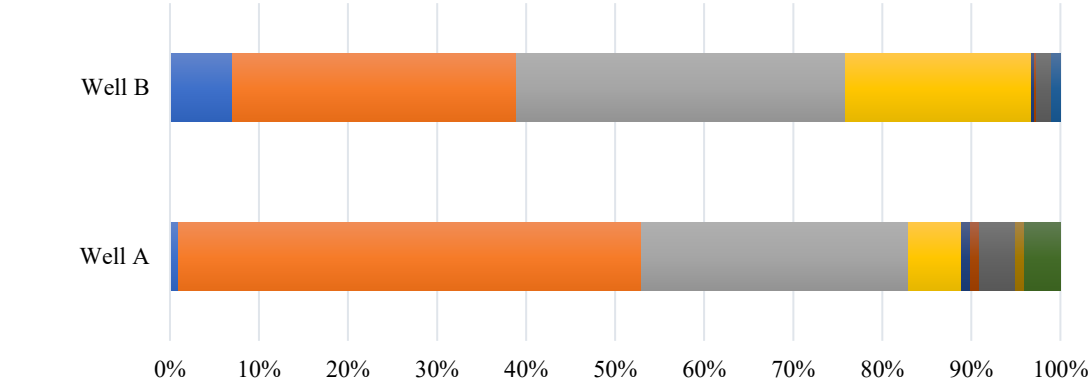
The integration of hyperspectral imaging in this workflow serves as a significant enhancement over conventional techniques, allowing for non-destructive, high-resolution, and spatially continuous characterization of the reservoir rock. This approach is especially beneficial in detecting mineral zoning, mixed clay phases, and alteration patterns that might be overlooked by point-based methods such as XRD or petrography (Bishop et al., 2011; Kokaly et al., 2017).

3. Results and Discussion

3.1. Formation Lithology Explorer (FLEX) Result

The FLEX log results provided an essential first insight into the mineralogical composition of the Devonian reservoirs in both wells. Although FLEX is a downhole tool with limited sensitivity to finely interbedded or dispersed clays, its preliminary identifications were particularly helpful in contextualizing the operational challenges encountered during drilling and testing.

For Well A, the FLEX results indicated a dominance of quartz (52%) and illite (30%), with minor components of smectite (6%), calcite (4%), and other trace minerals including kaolinite, dolomite, and sulphates (**Figure 6**). The significant illite content explains much of the reduced permeability observed during testing. Illite is known for its pore throat-clogging behavior and low swelling potential, which can reduce reservoir quality while maintaining structural stability. The presence of smectite, although lower, raises concerns about potential swelling and sensitivity to water-based fluids. However, in Well A, the use of oil-based mud (OBM) may have mitigated these effects. The relatively high quartz percentage also suggests a mechanically stable formation, though insufficient alone to ensure reservoir deliverability. These mineralogical characteristics, particularly the clay content, are consistent with the low production potential observed in the well, ultimately contributing to its abandonment decision.



	Well A	Well B
Kaolinite	1%	7%
Quartz	52%	32%
Illite	30%	37%
Smectite	6%	21%
Chlorite	0%	0%
Mica	0%	0%
Sulphate	1%	0%
Dolomite	1%	0%
Calcite	4%	2%
Fe-Carbonate	1%	0%
Ferrous-Index	0%	1%
Others	4%	0%

Figure 6 Formation Lithology Explorer (FLEX) Results for well A & B

In contrast, Well B shows a somewhat different mineralogical profile, with quartz at 32%, slightly higher illite at 37%, and a notably higher smectite content at 21% (**Figure 6**). Although the clay type is similar, the increased smectite concentration introduces additional risk of swelling and reduced permeability. These findings align with the moderate hydrocarbon inflow (~2.2 m^3) observed during testing, suggesting that despite some production, the reservoir quality remains constrained by clay-related permeability issues. The use of KCl-polymer drilling fluid, known for minimizing clay swelling, was a strategic choice in this well, though not entirely sufficient to overcome the formation's limitations.

The FLEX data, despite its limitations, thus offer a coherent narrative linking mineralogy to field performance. However, due to possible inaccuracies in the quantitative estimation of clay types and abundance, further validation is required. For this reason, X-ray Diffraction (XRD) and Hyperspectral Imaging analyses were planned and conducted.

3.2. XRD Results

The XRD analysis identified the main mineralogical components responsible for formation behavior in Wells A and B. The results highlight a high content of reactive clays, which explains several damage mechanisms previously detected by other tools.

The sample from Well A shows a dominance of kaolinite (65%), followed by quartz (20%), and smaller amounts of illite, smectite, and chlorite (5% each) (**Figure 7**). This composition indicates a formation with a high risk of clay dispersion and migration, particularly due to kaolinite's platy structure and tendency to detach under flow. Quartz offers some structural stability, reducing the severity of mechanical damage.

These mineralogical features explain the moderate permeability impairment observed previously: damage in Well A is mainly due to fines migration and partial pore blockage, but remains somewhat limited thanks to the stabilizing role of quartz.

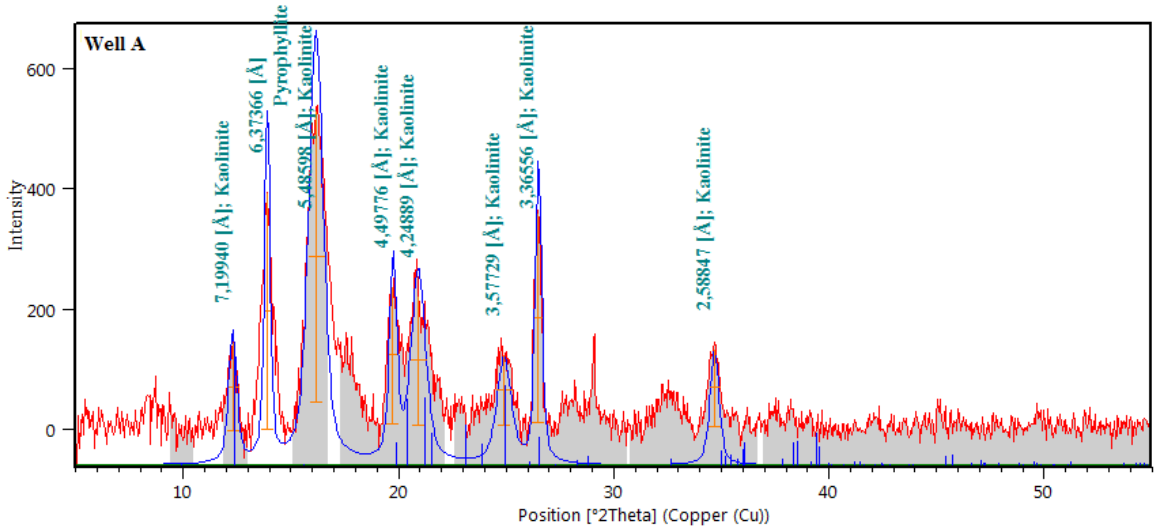


Figure 7 XRD Results for well A

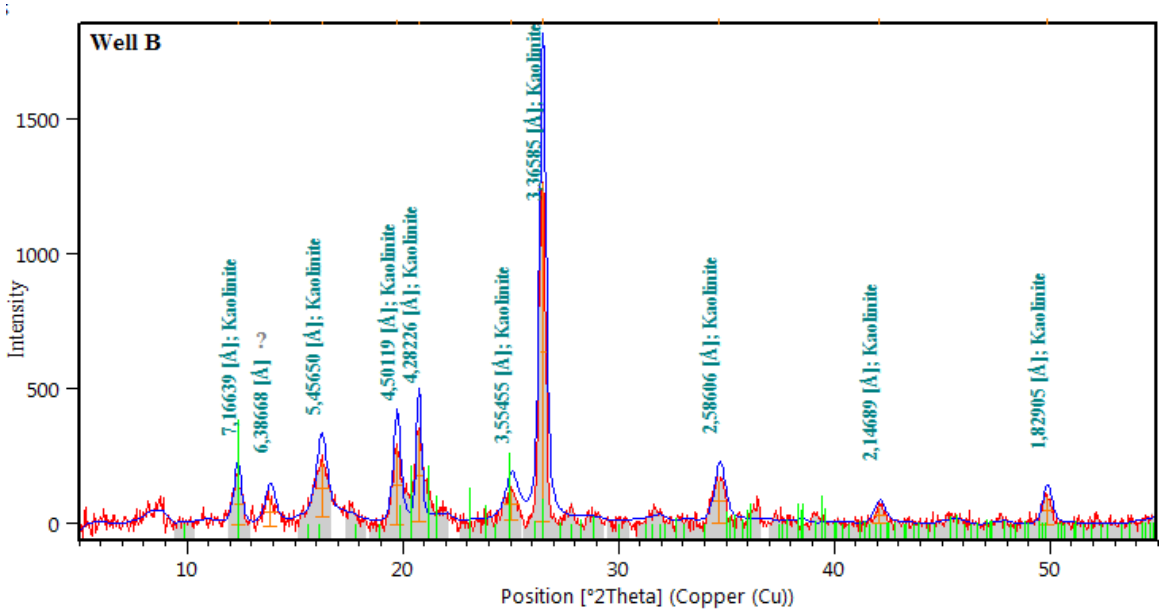
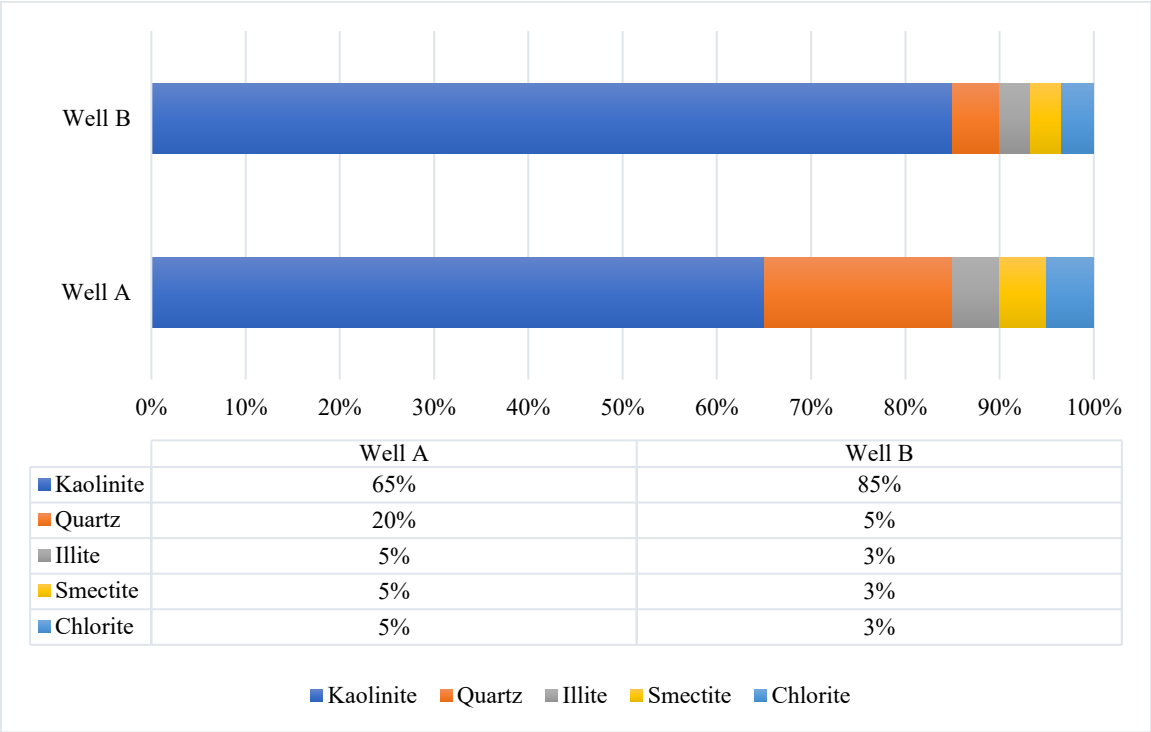


Figure 8 XRD Results for well b

In contrast, Well B contains 85% kaolinite and only 5% quartz, making the formation far more vulnerable (**Figure 9**). The very high clay content, combined with poor quartz support, makes the rock susceptible to extensive fines migration, pore throat plugging, and structural collapse. Even though illite, smectite, and chlorite are present in small quantities (3% each), their effect is amplified in a matrix already dominated by kaolinite.

This fully aligns with the severe mechanical and permeability damage detected in Well B using other diagnostic tools. The mineralogy points to a weak, highly reactive formation, likely to be damaged during fluid circulation or production.



	Well A	Well B
Kaolinite	65%	85%
Quartz	20%	5%
Illite	5%	3%
Smectite	5%	3%
Chlorite	5%	3%

Figure 9 XRD Results for well A & B

The analysis was conducted over a 2θ range sufficient to detect the key clay minerals (kaolinite, smectite, illite, chlorite). While minor minerals with overlapping signals may not be clearly resolved, the dominant phases were accurately identified, supporting the study's objective.

To confirm these findings and improve spatial understanding of mineral distribution, it is recommended to use Hyperspectral Imaging (HSI). HSI can help detect vertical variations and heterogeneities in clay content, which are crucial for designing appropriate treatment and mitigation strategies.

3.3. Hyperspectral Results

Hyperspectral Imaging (HSI) was employed to analyze the mineralogical composition of cores from Well A and Well B. Well A exhibits an unusually high mica content (42%), with kaolinite (12%) and minor illite (7%) and chlorite (2%) (**Figure 10**, **Figure 11**). Mica, known for its platy morphology and weak bonding, reduces the mechanical integrity of the rock matrix and contributes to borehole instability and sanding problems (Haneef et al., 2020).

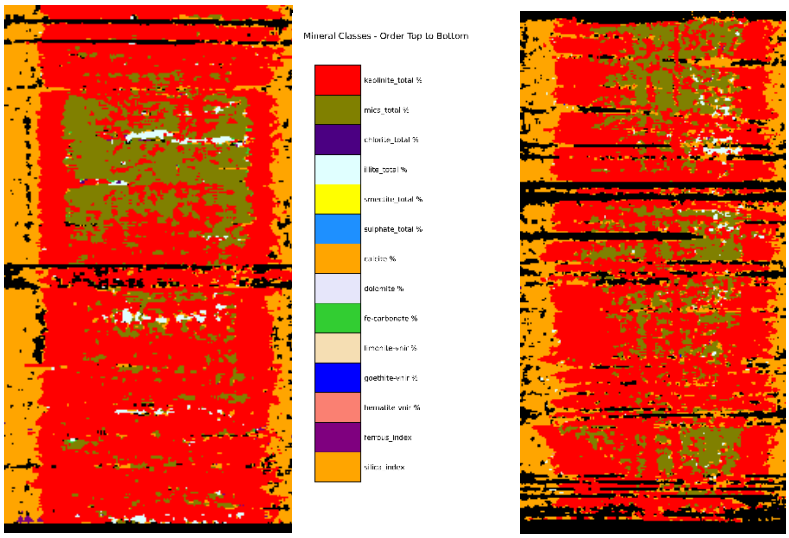
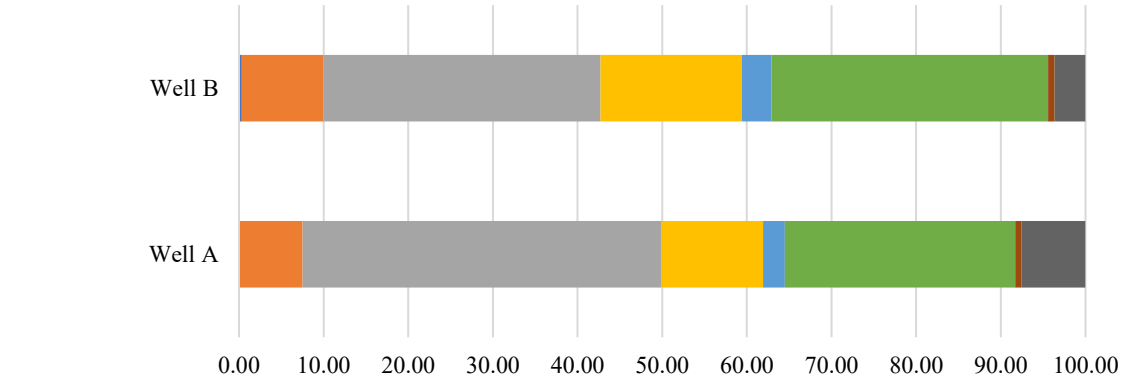


Figure 10 Mineral Composition Analysis of Gedinnean Core Sample from Well A & B: Percentage Distribution

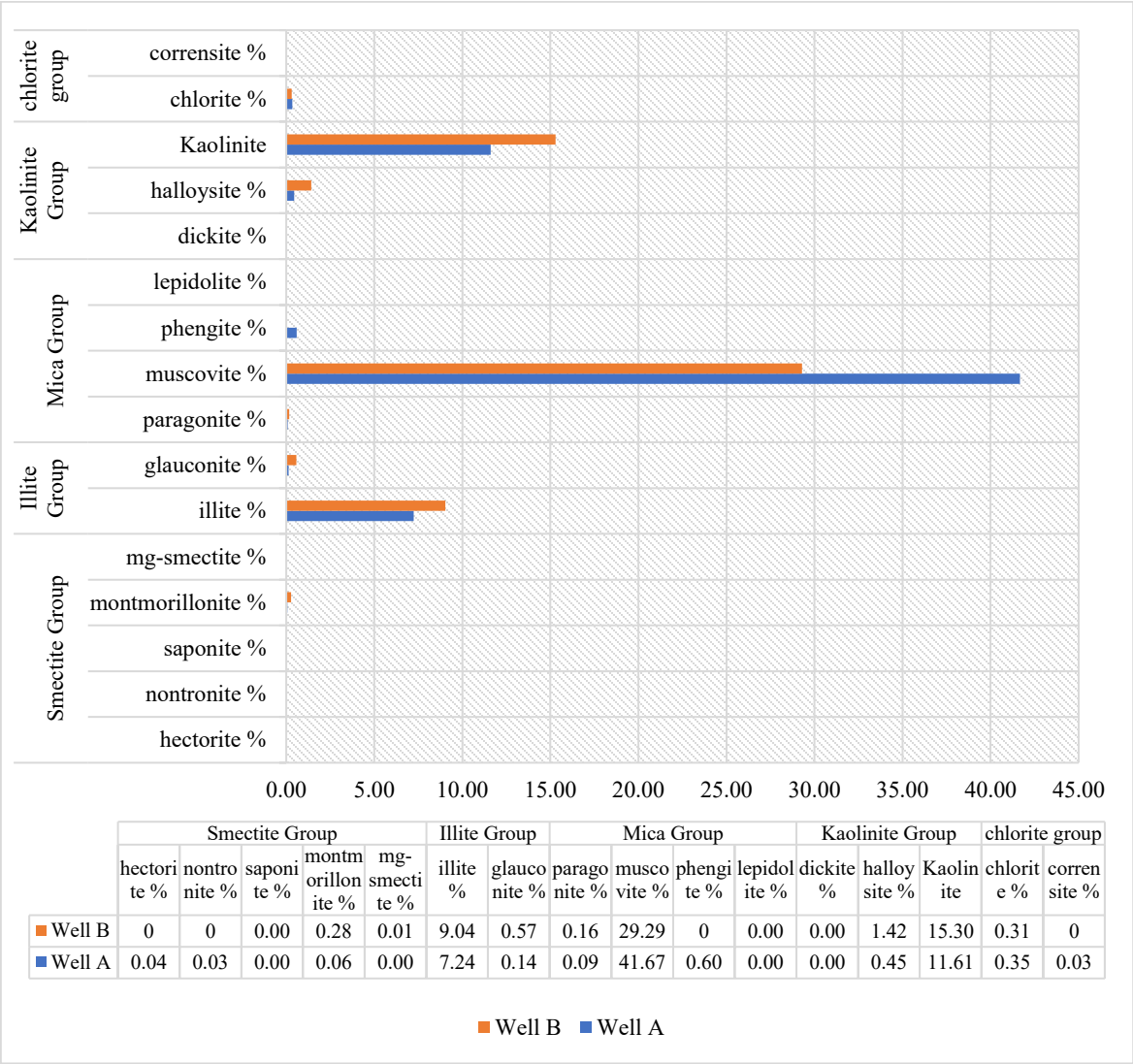
The high mica content is strongly correlated with wellbore collapse and excessive torque and drag observed during drilling operations in Well A. Kaolinite, although not as plastic as smectite, can still detach and migrate with fluids, contributing to pore throat plugging and permeability reduction. Kaolinite and mica alone are sufficient to explain the mechanical fragility and poor production performance observed in Well A.



	Well A	Well B
smectite_total %	0.13	0.34
illite_total %	7.38	9.62
mica_total %	42.35	32.75
kaolinite_total %	12.06	16.71
chlorite_total %	2.55	3.48
carbonate_total %	27.26	32.68
sulphate_total %	0.02	0.02
hydrocarbon_total %	0.67	0.76
Minor Minerals %	7.57	3.63

Figure 11 Hyperspectral Imaging (VNIR/SWIR Spectroscopy) Results for well A & B (%)

Well B presents a more complex mineral assemblage. While mica is still dominant (32%), its proportion is lower than in Well A. Kaolinite is slightly higher (16%), and illite is significantly increased (9%) (**Figure 10**, **Figure 11**). Illite and kaolinite are both prone to fines generation and migration, particularly under high-velocity or water-based fluid flow (Wilson et al., 2014), which could explain the decline in production rate and skin damage observed in Well B.



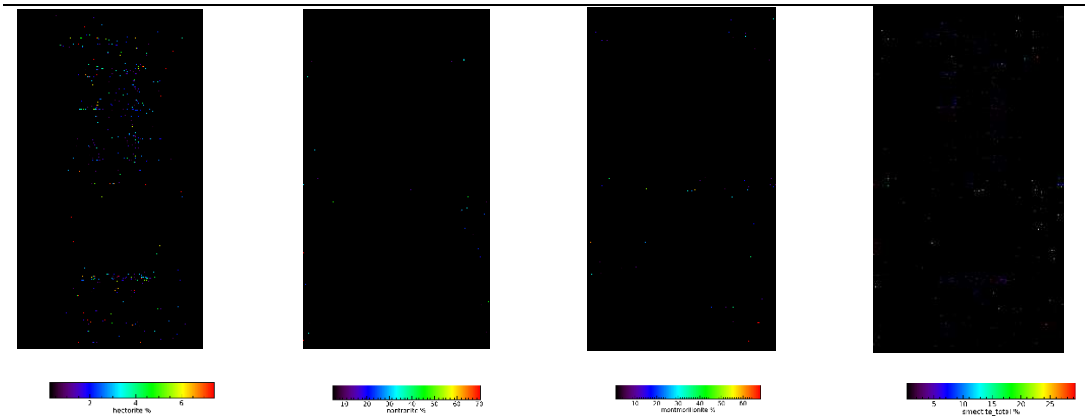
	Smectite Group					Illite Group		Mica Group				Kaolinite Group			chlorite group	
	hectorite %	nontronite %	saponite %	montmorillonite %	mg-smectite %	illite %	glauconite %	paragonite %	muscovite %	phengite %	lepidolite %	dickite %	halloysite %	Kaolinite	chlorite %	corrensite %
Well B	0	0	0.00	0.28	0.01	9.04	0.57	0.16	29.29	0	0.00	0.00	1.42	15.30	0.31	0
Well A	0.04	0.03	0.00	0.06	0.00	7.24	0.14	0.09	41.67	0.60	0.00	0.00	0.45	11.61	0.35	0.03

Figure 12 Clay total HSI results for Well A and B

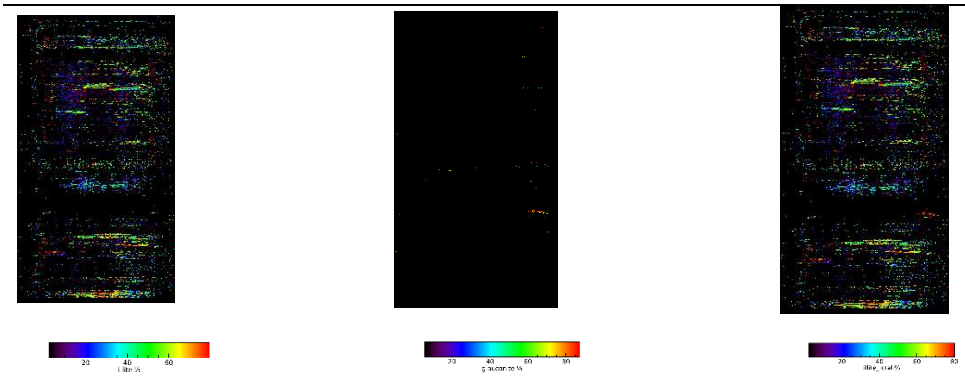
The presence of calcite (6%) suggests a possible contribution to chemical instability (**Figure 12**), especially in the presence of acidic fluids during stimulation or cementing. Dissolution or precipitation of calcite can alter porosity and further reduce permeability (Civan, 2007).

Although the mechanical issues in Well B are less severe than those in Well A, the combination of high clay content and chemical sensitivity points to a different type of damage: combined mechanical and chemical formation damage leading to reduced injectivity or productivity.

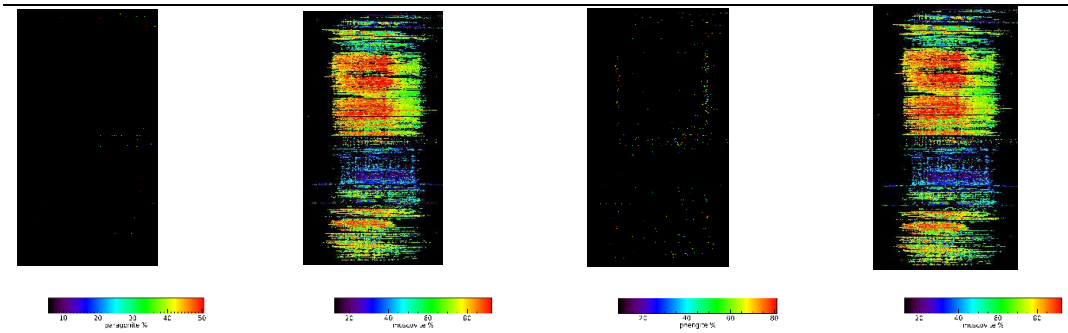
Smectite



Illite



Mica



Kaolinite **Chlorite**

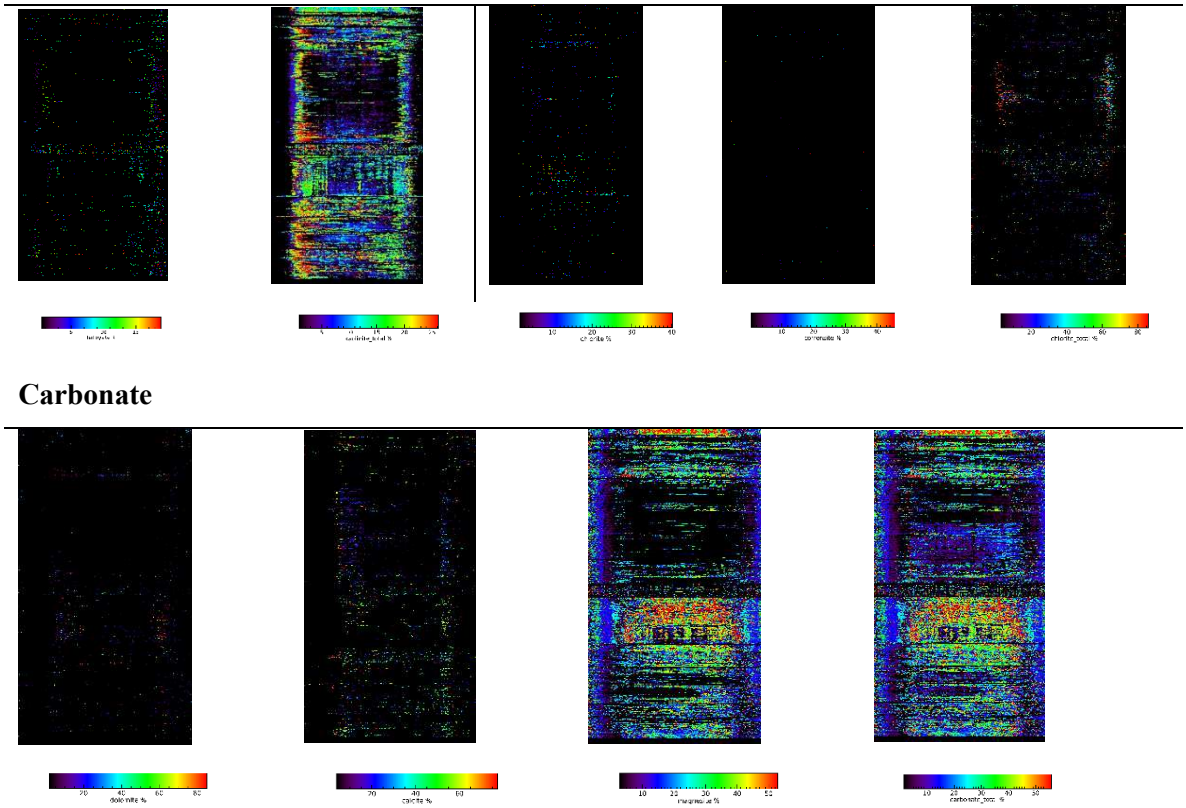
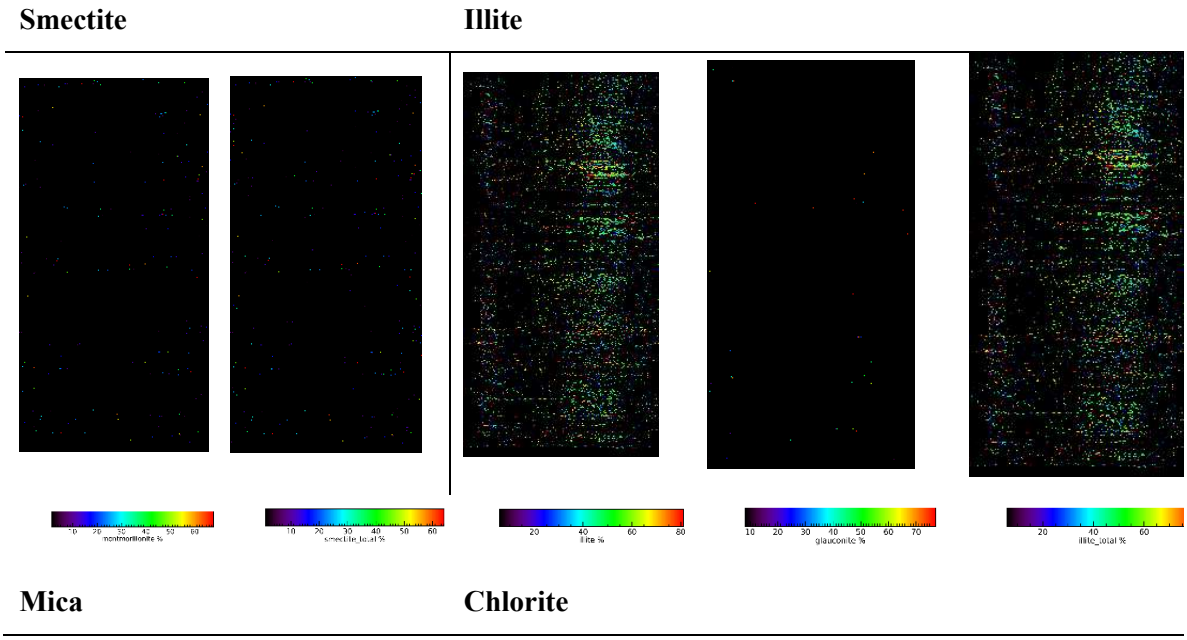
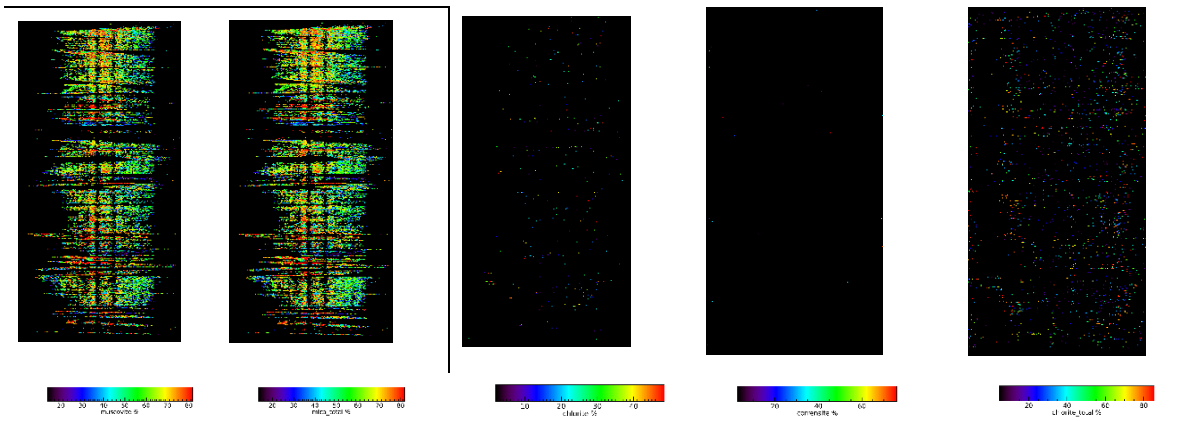
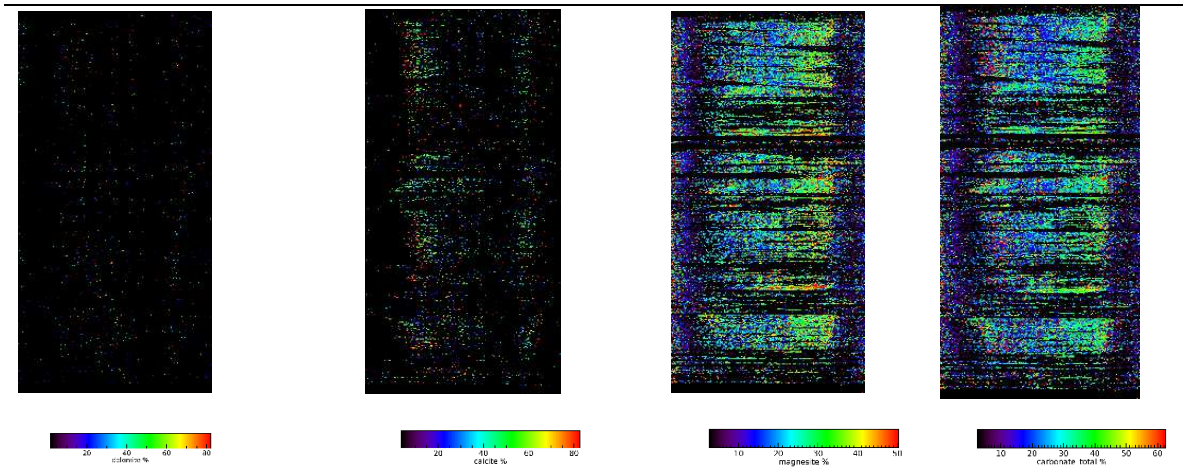


Figure 13 HSI Results detailled results for Well A





Carbonate



Kaolinite



Figure 14 HSI Results detailled results for Well B

3.4. Integrated Comparison of FLEX, XRD, and HSI Results

The combined application of FLEX logging, XRD mineral quantification, and Hyperspectral Imaging (HSI) constitutes a robust framework for diagnosing clay-related formation issues in Wells A and B. Drawing on insights from published studies such as HSI's ability to detect clays invisible to XRD in low concentrations (Murphy et al., 2017) and the special significance of mica and kaolinite features in SWIR spectra (Clark et al., 1990; Kruse et al., 2014) this multimodal approach reveals a comprehensive picture of reservoir behavior.

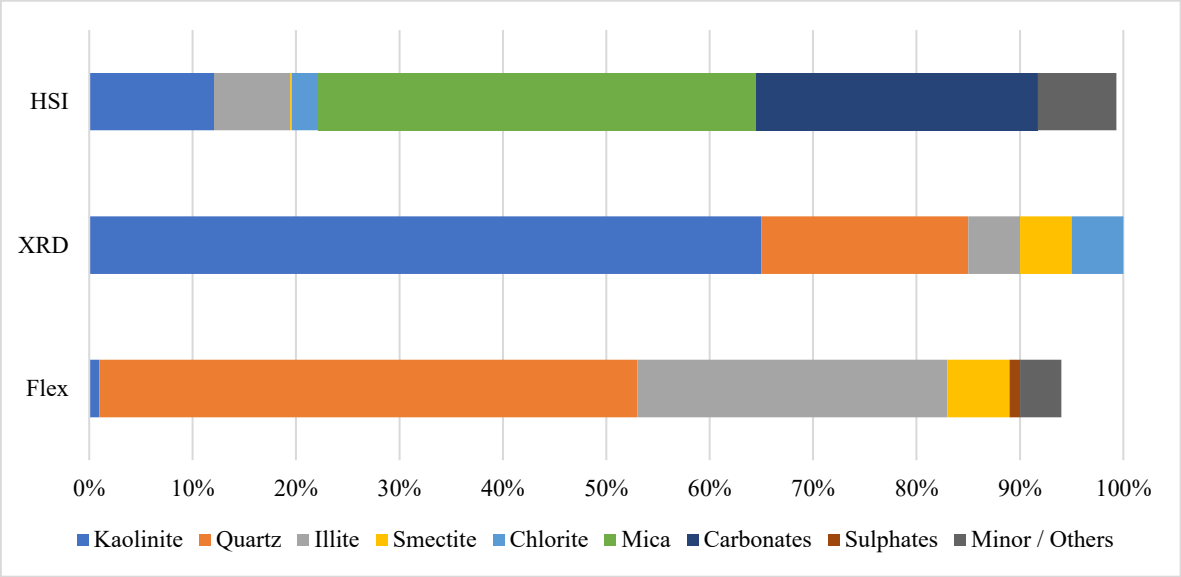


Figure 15 FLEX, XRD and HSI results for Well A

In Well A, FLEX logs indicated persistent clay-rich zones, alerting to risk of swelling and reduced permeability. XRD analysis quantified major kaolinite at 65%, supported by modest contributions from quartz (20%) and minor illite, smectite, and chlorite (5% each). High kaolinite content explains fines migration and permeability compaction. HSI results, however, revealed a dominant mica content (42%), with kaolinite (12%) and minor illite and chlorite, highlighting mechanical fragility due to mica's flaky structure.

Despite FLEX and XRD identifying kaolinite as the main culprit behind poor production, HSI clarified that mica was the principal driver of mechanical instability (**Figure 14**). This interpretive refinement aligned with studies showing that spectral dominance of mica can mask other clays (Bishop et al., 2008) explains the severe drilling and productivity issues experienced in Well A.

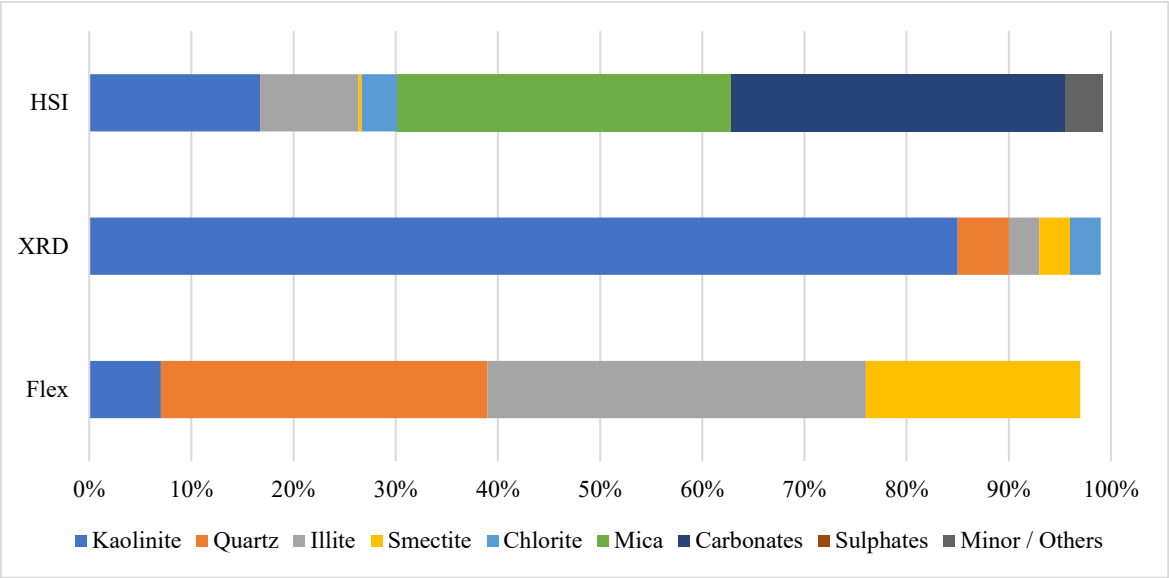


Figure 16 FLEX, XRD and HSI results for Well B

In Well B, FLEX logs detected clay zones of intermediate severity. XRD results dramatically showed 85% kaolinite, with only 5% quartz and minor illite, smectite, chlorite (3% each). This suggested kaolinite-induced migration and plugging. HSI, however, indicated that while kaolinite remains high (16%), mica represents 32%, and illite is significantly higher (9%), with notable calcite (6%).

Unlike Well A, HSI here exposes a dual damage mechanism for Well B kaolinite and illite migration combined with mechanical weakening from mica, and chemical sensitivity from calcite (**Figure 15**). This multilayered pathology explains production decline and skin damage, as observed in operational logs.

This multipronged approach validates the weaknesses observed in Wells A and B with data-driven explanations: mica dominance and high kaolinite content in Well A, and combined kaolinite-illite migration with calcite sensitivity in Well B. The study demonstrates that HSI is a powerful enhancement to traditional tools, offering both strategic and practical improvements in subsurface reservoir characterization.

4. General conclusion

This study evaluated the application of hyperspectral imaging (HSI) in combination with Formation Lithology Explorer (FLEX) logging and X-ray diffraction (XRD) for mineralogical

characterization of clay-rich Devonian reservoirs in the El Ouabed region, Algeria. The comparison was performed on selected core intervals from two wells targeting the Gedinnean reservoir.

The three techniques provided complementary information, while also showing significant differences in the estimated mineral abundances. FLEX provided continuous downhole mineralogical information and identified clay-rich intervals, whereas XRD provided direct identification of crystalline mineral phases in the analyzed samples. HSI provided high-resolution spatial information and identified a broader assemblage of spectrally active minerals, including mica, kaolinite, illite and chlorite.

For Well A, FLEX indicated a quartz- and illite-dominated mineralogical profile, whereas XRD indicated a predominantly kaolinitic assemblage. HSI identified abundant mica together with kaolinite and illite. For Well B, the three methods again produced different mineralogical proportions, with XRD indicating a strongly kaolinitic composition, while HSI identified significant contributions from mica, kaolinite and illite. These differences highlight the fact that mineral abundance estimates are dependent on the analytical technique, its sensitivity, spatial scale and sample preparation.

The results therefore support the use of HSI as a complementary technique rather than as a replacement for conventional mineralogical and logging methods. Its main advantage in the present study is its ability to provide high-resolution spatial mapping of mineralogical variability along the analyzed core intervals. When integrated with XRD and FLEX, this information can improve the interpretation of clay-rich intervals and provide additional constraints for evaluating potential formation-damage mechanisms.

The mineralogical assemblages identified in the two wells are consistent with several potential reservoir-quality and drilling concerns, including fines migration, pore-throat plugging and clay-related sensitivity. However, the present dataset is limited to two one-metre core intervals, and the observed mineralogical differences should therefore be interpreted as site-specific observations rather than as representative mineralogical distributions for the entire El Ouabed field.

Recommendations

Future work should extend the HSI–XRD–FLEX comparison to a larger number of core intervals and wells in order to evaluate the reproducibility of the observed mineralogical patterns. Independent validation using complementary techniques such as petrographic microscopy, SEM–

EDS or FTIR would also help constrain the interpretation and improve confidence in the semi-quantitative HSI results.

The integration of high-resolution HSI mineralogical maps with conventional well logs and laboratory mineralogical analyses could subsequently be incorporated into reservoir characterization workflows, particularly in clay-rich formations where mineralogical heterogeneity may influence drilling-fluid selection, formation damage and reservoir performance.

Overall, the study demonstrates the potential of hyperspectral core imaging as a rapid, non-destructive and spatially resolved complementary tool for mineralogical characterization of clay-rich petroleum reservoirs, while emphasizing the importance of multimodal validation for reliable quantitative interpretation.

Acknowledgements

Funding was provided by Faculty of Hydrocarbon and Chemistry, University M'Hamed Bougara Boumerdes, Algeria
faculty of hydrocarbons, renewable energies, and earth and universe sciences, Kasdi Merbah university of Ouargla, Algeria.

Conflict of interest statement

Conflict of interest On behalf of all authors, the corresponding author states that there is no conflict of interest.

References

- Berger, Z., Ross, D. J. K., & Mason, P. J. (2019). Application of Hyperspectral Imaging in Tight Sandstone Reservoirs. *AAPG Bulletin, 103*(4), 765–784.
- Bish, D. L., & Post, J. E. (1989). *Modern Powder Diffraction*. Reviews in Mineralogy, Volume 20. Mineralogical Society of America.
- Bishop, J. L., Madejová, J., Komadel, P., & Fröschl, H. (2008). The influence of structural Fe, Al and Mg on the infrared spectra of dioctahedral smectites. *Clay Minerals, 43*(1), 35–54. https://doi.org/10.1180/claymin.2008.043.1.03
- Chilingar, G. V., & Vorabutr, P. (1981). *Drilling and Drilling Fluids*. Elsevier.

- Clark, R. N., King, T. V. V., Klejwa, M., Swayze, G. A., & Vergo, N. (1990). High spectral resolution reflectance spectroscopy of minerals. *Journal of Geophysical Research: Solid Earth, 95*(B8), 12653–12680. https://doi.org/10.1029/JB095iB08p12653

- Clark, R. N., et al. (2003). Imaging spectroscopy: Earth and planetary remote sensing with the USGS Tetracorder and expert systems. *Journal of Geophysical Research: Planets, 108*(E12).

- Civan, F. (2007). *Reservoir Formation Damage*. Gulf Professional Publishing.

- El-Toukhy, A., Hammuda, O., & Hamouda, A. (2013). Clay Mineral Impact on Reservoir Permeability in North African Devonian Sandstones. *Journal of Petroleum Geology, 36*(3), 257–268.

- Gale, J. F. W., Elliott, S. J., & Holder, J. (2017). Using hyperspectral core imaging to evaluate fracture-filling mineralogy in shale gas plays. *Marine and Petroleum Geology, 86*, 1101–1111.

- Gardner, R. P., Pevey, R. E., & Verghese, K. (1997). Gamma-ray spectroscopy for elemental analysis in well logging. *Applied Radiation and Isotopes, 48*(10–12), 1453–1461.

- Grau, J. A., & Schweitzer, J. S. (1990). A new thermal neutron capture cross section logging system. *SPE Formation Evaluation, 5*(4), 401–408.

- Haneef, M., Rehman, M., & Khan, M. (2020). Borehole instability in mica-rich shales. *Journal of Petroleum Science and Engineering, 184*, 106488.

- Kruse, F. A., Boardman, J. W., & Huntington, J. F. (2014). Comparison of airborne hyperspectral data and EO-1 Hyperion for mineral mapping. *IEEE Transactions on Geoscience and Remote Sensing, 52*(5), 3051–3060. https://doi.org/10.1109/TGRS.2013.2267747

- Moore, D. M., & Reynolds, R. C. (1997). *X-ray Diffraction and the Identification and Analysis of Clay Minerals* (2nd ed.). Oxford University Press.

- Murphy, R. J., Schneider, S., & Monteiro, S. T. (2017). Mapping clay minerals in rock outcrops using hyperspectral and LiDAR data fusion. *Remote Sensing, 9*(7), 690. https://doi.org/10.3390/rs9070690

- Pittman, E. D. (1992). Relationship of porosity and permeability to various parameters derived from thin section and SEM images. *Journal of Sedimentary Research, 62*(3), 537–546.

- Quirein, J., Trantham, E., & El-Zehairy, A. (2007). Advanced log analysis for clay typing in complex reservoirs. *SPWLA 48th Annual Logging Symposium*.
- Ramezanianpour, A. A., Pilvar, A., & Mahdikhani, M. (2012). Use of XRD and SEM to study hydration products in cement-based materials. *Cement and Concrete Research, 42*(4), 595–604.
- Rider, M., & Kennedy, M. (2011). *The Geological Interpretation of Well Logs*. Rider-French Consulting.
- Środoń, J. (1984). X-ray powder diffraction identification of illite and mixed-layer illite/smectite. *Clays and Clay Minerals, 32*(5), 337–349.
- Turner, A. (2014). Hyperspectral imaging of drill core for mineral exploration. *Proceedings of Exploration 17*, 421–433.
- Wilson, M. J., & Pittman, E. D. (1977). The effect of clay minerals on porosity and permeability in sandstone reservoirs. *Clay Minerals, 12*(3), 287–308.
- Wilson, M. J., Wilson, L., & Manning, D. A. C. (2014). Clay mineralogy and shale instability: A review. *Earth-Science Reviews, 132*, 57–71.

Annex

Table 1 stratigraphic succession of El Ouabed region

	Devonian	**Devonian**	**Devonia**	**Silurian**	**Ordovician**
Reservoir	**Emsian**	**Siegenian**	**Gedinnean**		
Thickness	**2689m to 3018m**	**3018m to 3272m**	**3272m-3321m**	**3321m to 3489m**	**3489m to 3540m**

Description	Clay: Gray to greenish-gray, light gray, reddish-brown, soft to indurated, silty, with traces of white to greenish-white silt, slightly dolomitic, and intervals of white to gray-white, microcrystalline, sandy, friable to moderately hard limestone. Anhydrite: White, powdery. Sandstone: White to gray-white, fine to very fine, siliceous, moderately consolidated to friable, rarely pyritic, hard, locally light gray, very fine	Sandstone: White, clayey, very fine to fine, friable, locally light gray, very fine to fine, rounded to sub-rounded, siliceous, silico-argillaceous, hard, carbonate-rich at the base, moderately hard to well-consolidated. Clay: Gray to light gray, dark gray, blackish, soft to indurated, micaceous, silty, with intercalations of white to gray, light gray, very	White to brown to dark gray sand- stone, transitioning to siltstone, very fine to fine, silico-argilla-ceous, moderately consolidated to friable, sub- angular to sub-rounded, with intervals of gray to light gray, soft to indurated, silty clay. Gray to light gray, reddish-brown clay with intervals of soft white limestone.	Gray to light gray to reddish-brown clay, silty, soft, slightly carbonate-rich, with intervals of white to off-white, soft, clayey limestone. Siltstone to very fine to fine white sandstone, occasion-ally blackish, clay-carbonate, mod-erately hard. Gray clay,	Sandstone: White to gray-white, very fine, clayey, moderately consolidated to well-consolidated, pyritic. Presence of rounded to sub-rounded quartz grains. Clay: Gray to light gray, gray-brown, occasionally green, soft to indurated, locally dark gray, pasty, soft to indurated, micaceous, silty to highly silty. Silt: Gray-white to dark gray

	to fine, sub-angular to sub-rounded, silico-argillaceous, friable to moderately hard, with fine intervals of light gray clay, soft to indurated, silty.	fine to fine, rounded to sub-rounded, silico-argillaceous, hard sandstone.		indurated, silty, carbonate -rich, finely mica-ceous, traces of limestone.	

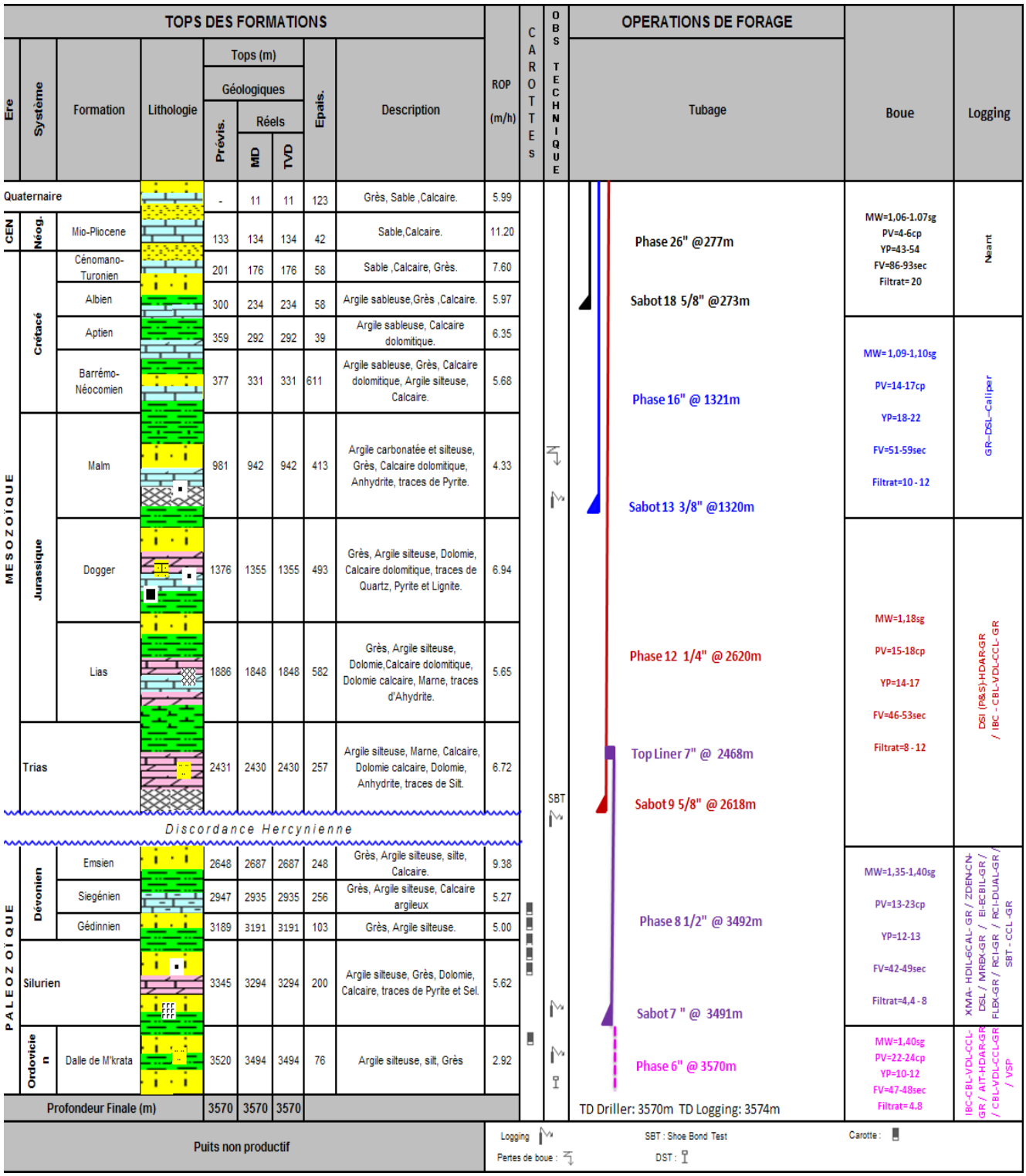


Figure 30 Technical Data Sheet of Well A

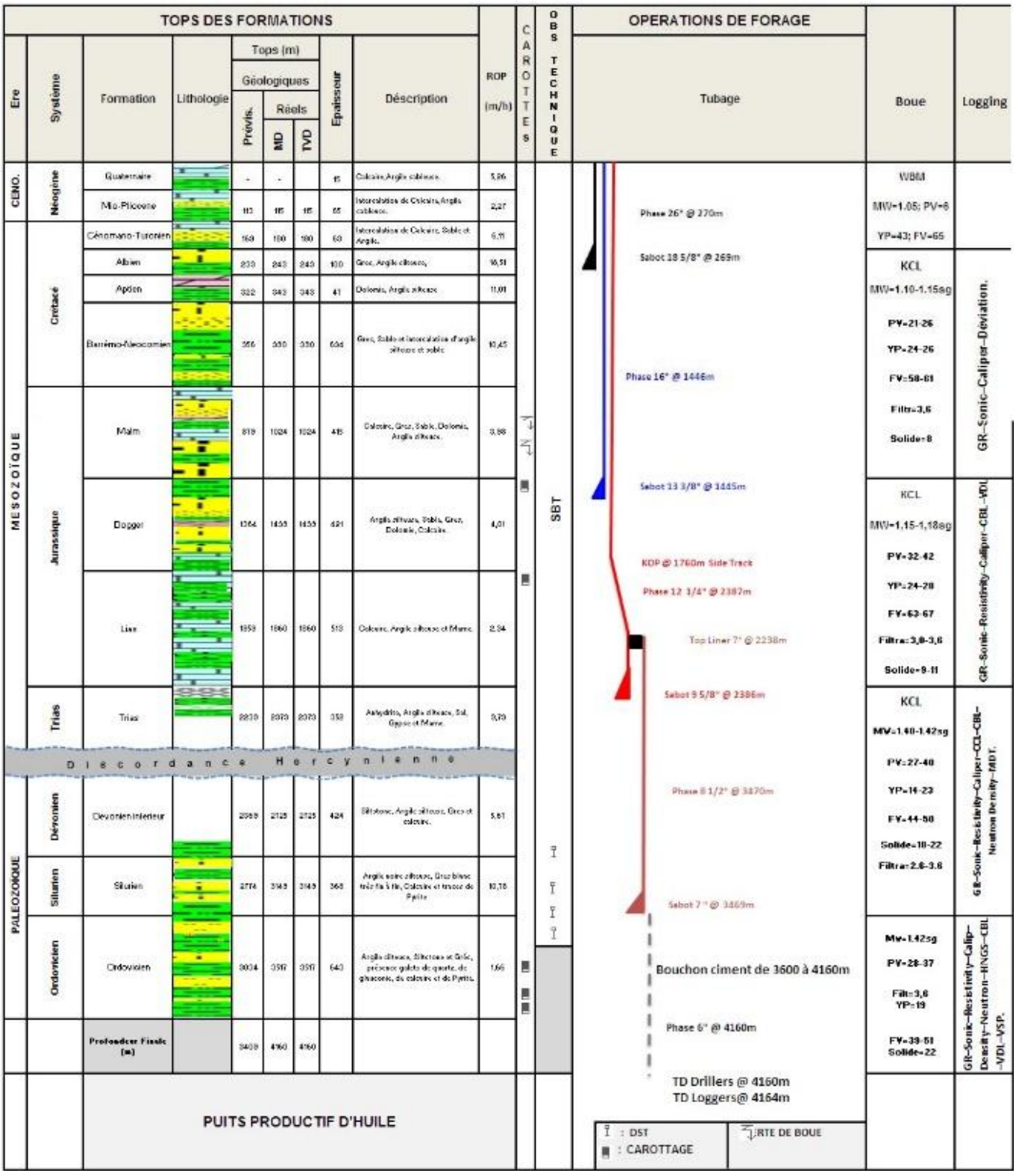
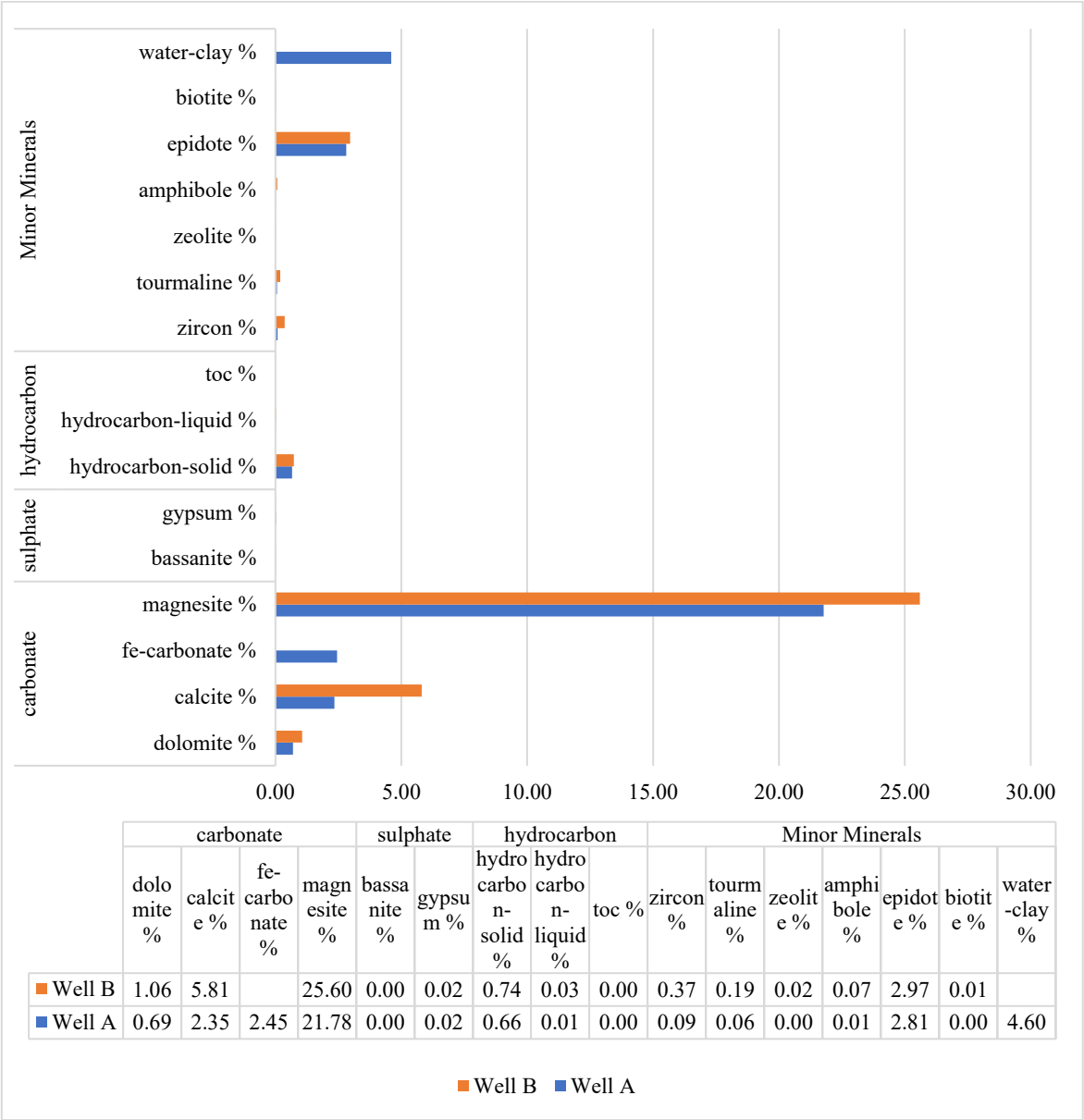


Figure 31 Technical Data Sheet of Well B



	carbonate				sulphate		hydrocarbon			Minor Minerals						
	dolomite %	calcite %	fe-carbonate %	magnesite %	bassanite %	gypsum %	hydrocarbon-solid %	hydrocarbon-liquid %	toc %	zircon %	tourmaline %	zeolite %	amphibole %	epidote %	biotite %	water-clay %
Well B	1.06	5.81		25.60	0.00	0.02	0.74	0.03	0.00	0.37	0.19	0.02	0.07	2.97	0.01	
Well A	0.69	2.35	2.45	21.78	0.00	0.02	0.66	0.01	0.00	0.09	0.06	0.00	0.01	2.81	0.00	4.60